## Supplemental figure legends

### Figure S1

Volcano plot showing that the background binding profiles of control beads and anti-GFP beads are very similar in worms that do not express GFP fusion proteins. Proteins cross-reactive to the anti-GFP beads (highlighted in red) were filtered out from the results of pull-down assays with GFP fusion proteins.

### Figure S2

**Pull-down simulation benchmark experiment.** To simulate the detection of label-free pull-down enrichment in a complex non-specific background, two predefined samples were measured in succession in triplicate. Sample 1: 1X *E. coli* lysate, 1X UPS2 human standard, recombinant CDC42; Sample 2: 1X *E. coli* lysate, 4X UPS2 human standard, recombinant RAC1, RHOA and GFP. A combined threshold (hyperbolic curves) was set based on a modified *t*-statistic ($s_0$ = 1.5, $t_0$ = 0.8).

### Figure S3

**Validation of CAR-1 interaction partners by co-immunoprecipitation and Western blotting.** Three examples demonstrating specific binding of GFP::CAR-1 to CAR-1, IFET-1, and SPN-4 proteins in experimental but not control pulldowns. Gamma-Tubulin was a non-specific background binder in the N2 pull-downs.

### Figure S4

**High-resolution embryo IVI map with protein names.**

**Figure S5**

**Depletion of *gei-12* by RNAi disrupts P granule formation in N2 early embryos.** Knocking down the paralogs of *gei-12* individually by RNAi in N2 embryos did not impair P granule assembly. Fixed embryos were stained with K76 antibody against P granules.

**Figure S6**

**Depletion of *gei*-12 by RNAi does not affect asymmetric localization of some other known P granule components (CAR-1, PIE-1, POS-1 and SPN-4) during early embryogenesis.**

**Figure S7**

***GEI-12* and its paralogs play partially redundant roles in P granule assembly.** Strains harboring mutations in *gei-12* (*tm4259* or *tm4526*) and its paralog *C36C9.1* (*tm4343*) were fixed and stained with K76 antibody against P granules, without or with RNAi against each member of the *gei-12* family. The P granule phenotype elicited by *gei-12(RNAi)* was considerably weaker in the two *gei-12* mutant backgrounds than in wild type (Fig. S5). RNAi against either *gei-12* paralog affected the P granule phenotype of *gei-12* mutants to variable extents, but had no obvious effect in the *tm4343* mutant background or in wild type (Fig. S5). The apparent lower penetrance of the *gei-12(RNAi)* phenotype in the *gei-12(tm4259)* and *gei-12(tm4526)* mutants may be due to different genetic backgrounds and/or the generally high variability of RNAi experiments and P granule phenotypes that were also observed by Wang et al., 2014.

Figure S1

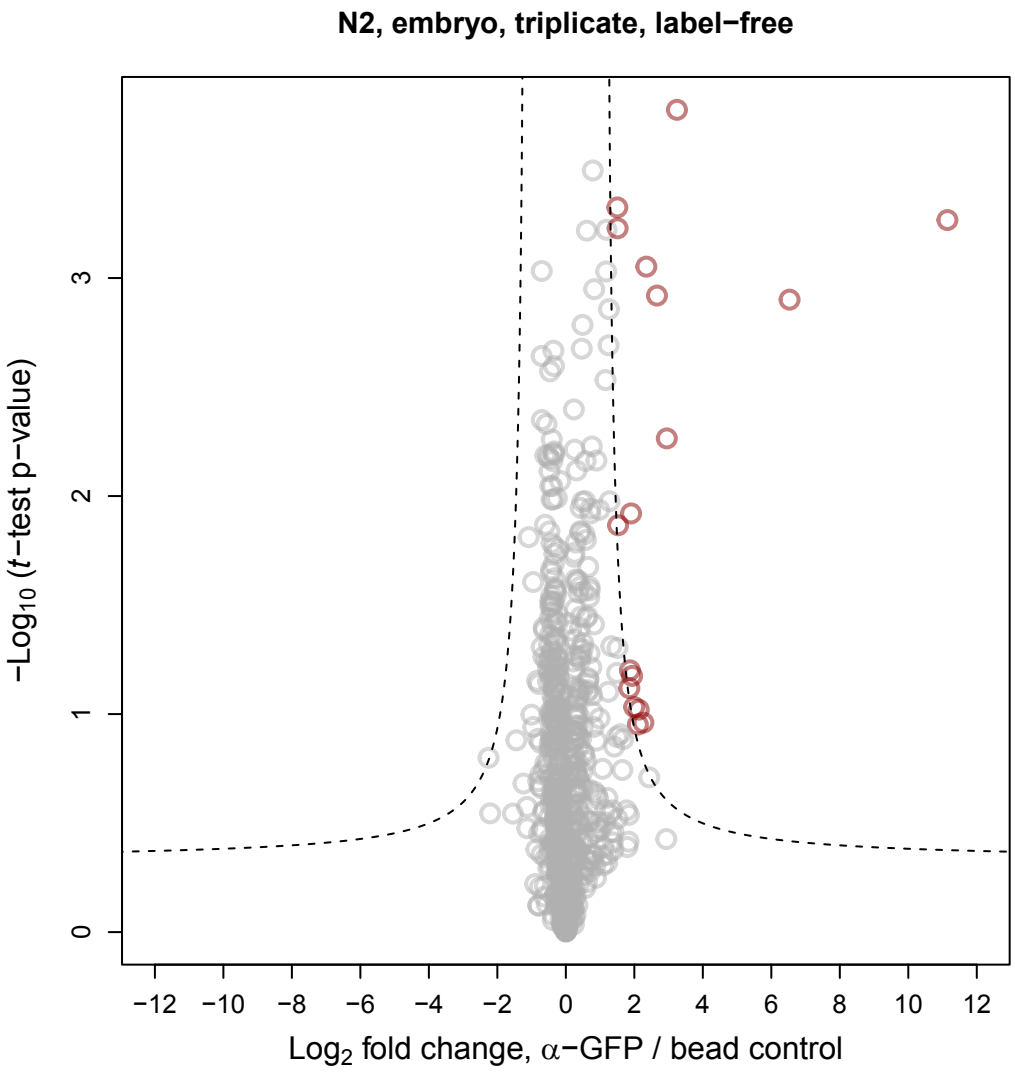
N2, embryo, triplicate, label−free
−Log10 (t−test p−value)
0
1
2
3
−12
−10
−8
−6
−4
−2
0
2
4
6
8
10
12
Log2 fold change, α−GFP / bead control

Figure S2

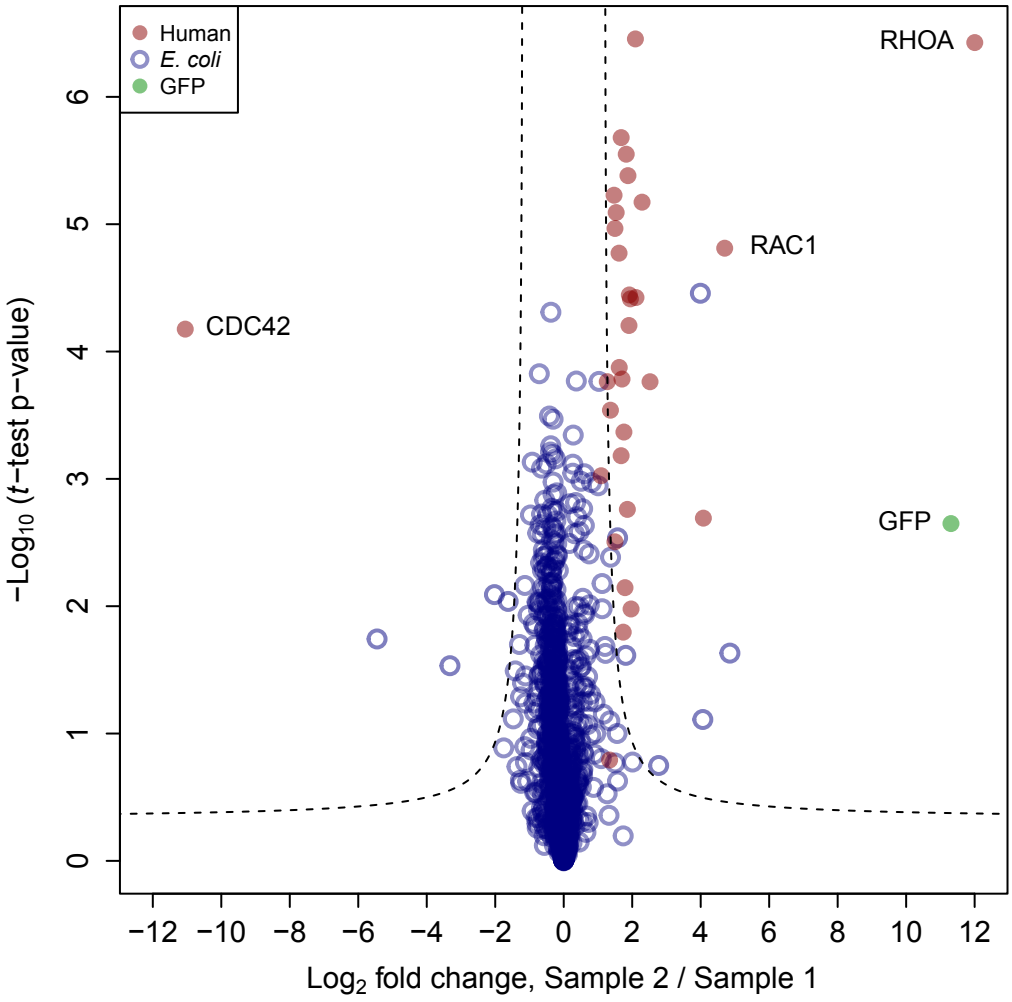
Human
E. coli
GFP
RHOA
RAC1
CDC42
GFP
−Log10 (t−test p−value)
Log2 fold change, Sample 2 / Sample 1
0
1
2
3
4
5
6
−12
−10
−8
−6
−4
−2
0
2
4
6
8
10
12

Figure S3

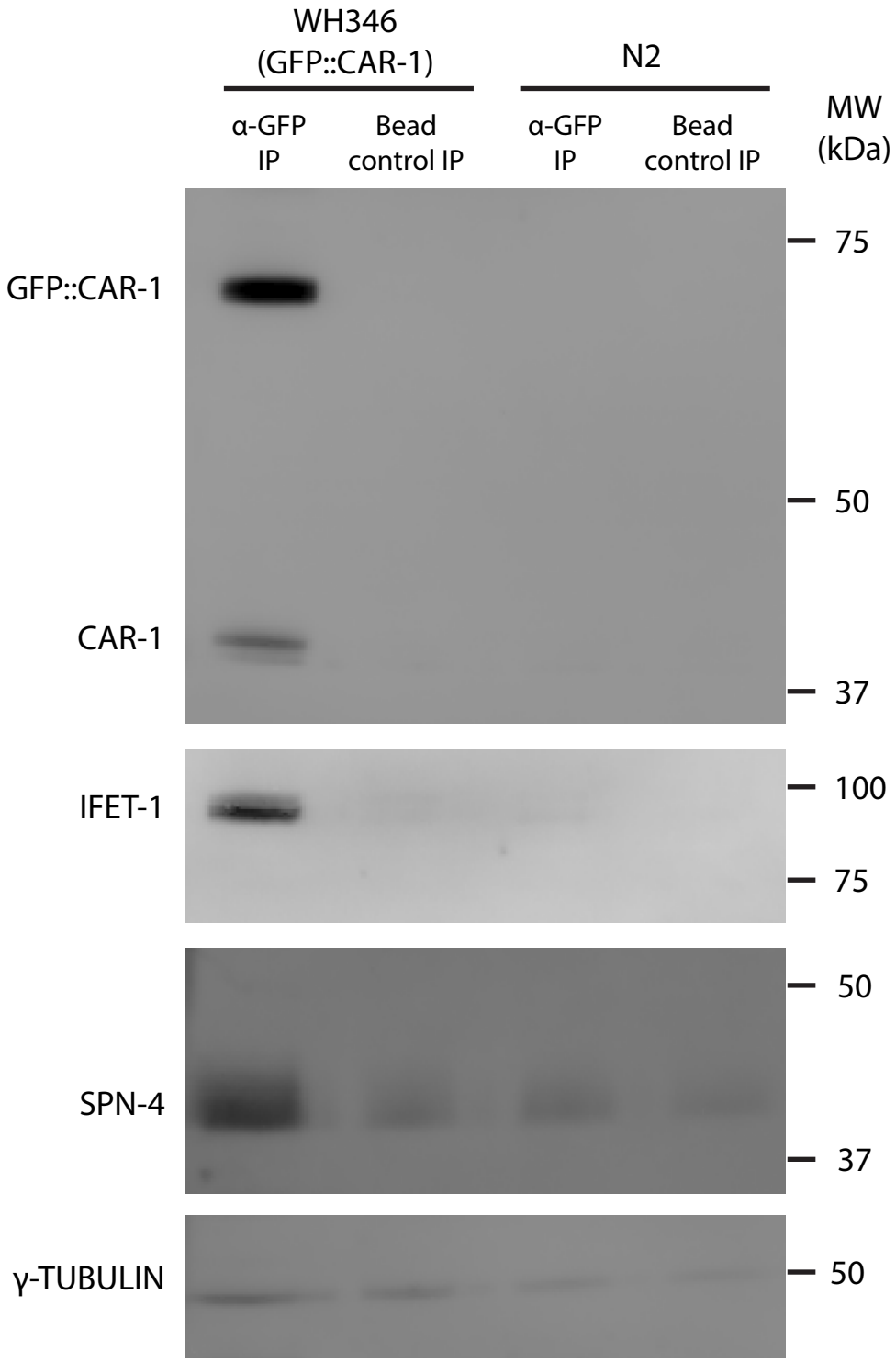
WH346
(GFP::CAR-1)
N2
α-GFP IP
Bead control IP
α-GFP IP
Bead control IP
MW (kDa)
GFP::CAR-1
CAR-1
IFET-1
SPN-4
γ-TUBULIN
75
50
37
100
75
50
37
50

# Figure S4

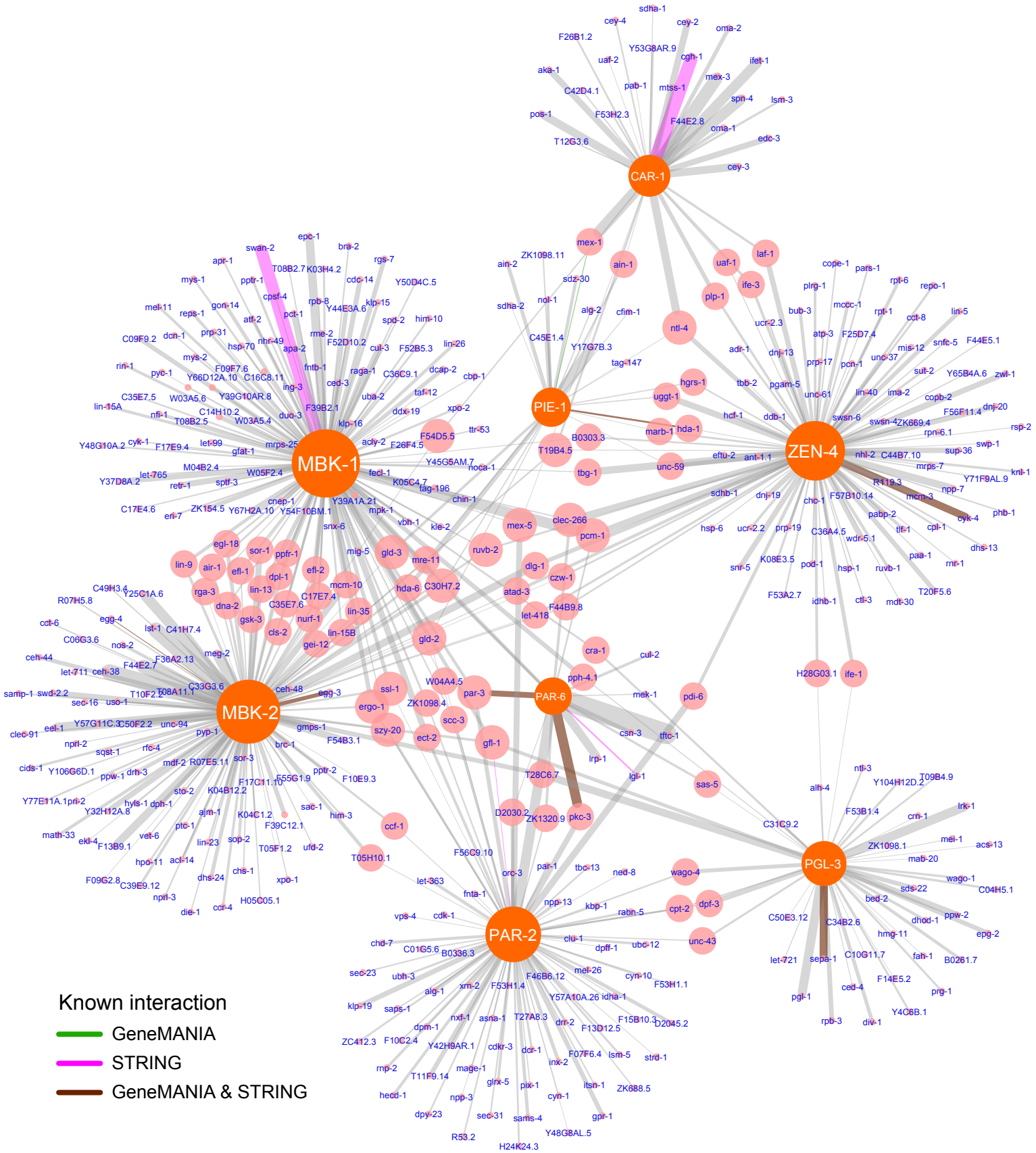
CAR-1
PIE-1
MBK-1
ZEN-4
MBK-2
PAR-6
PAR-2
PGL-3
Known interaction
GeneMANIA
STRING
GeneMANIA & STRING

Figure S5

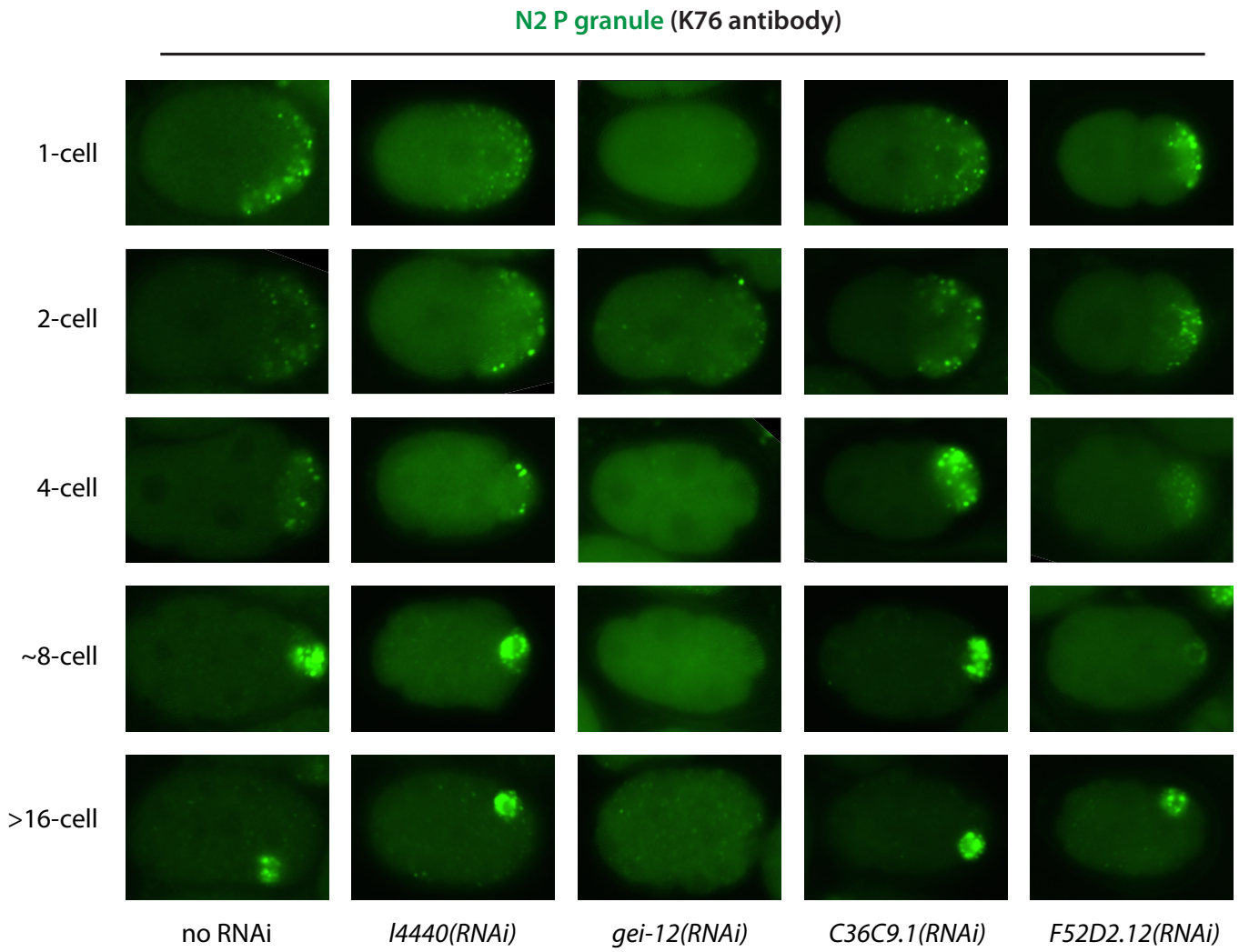
N2 P granule (K76 antibody)
1-cell
2-cell
4-cell
~8-cell
>16-cell
no RNAi
l4440(RNAi)
gei-12(RNAi)
C36C9.1(RNAi)
F52D2.12(RNAi)

# Figure S6

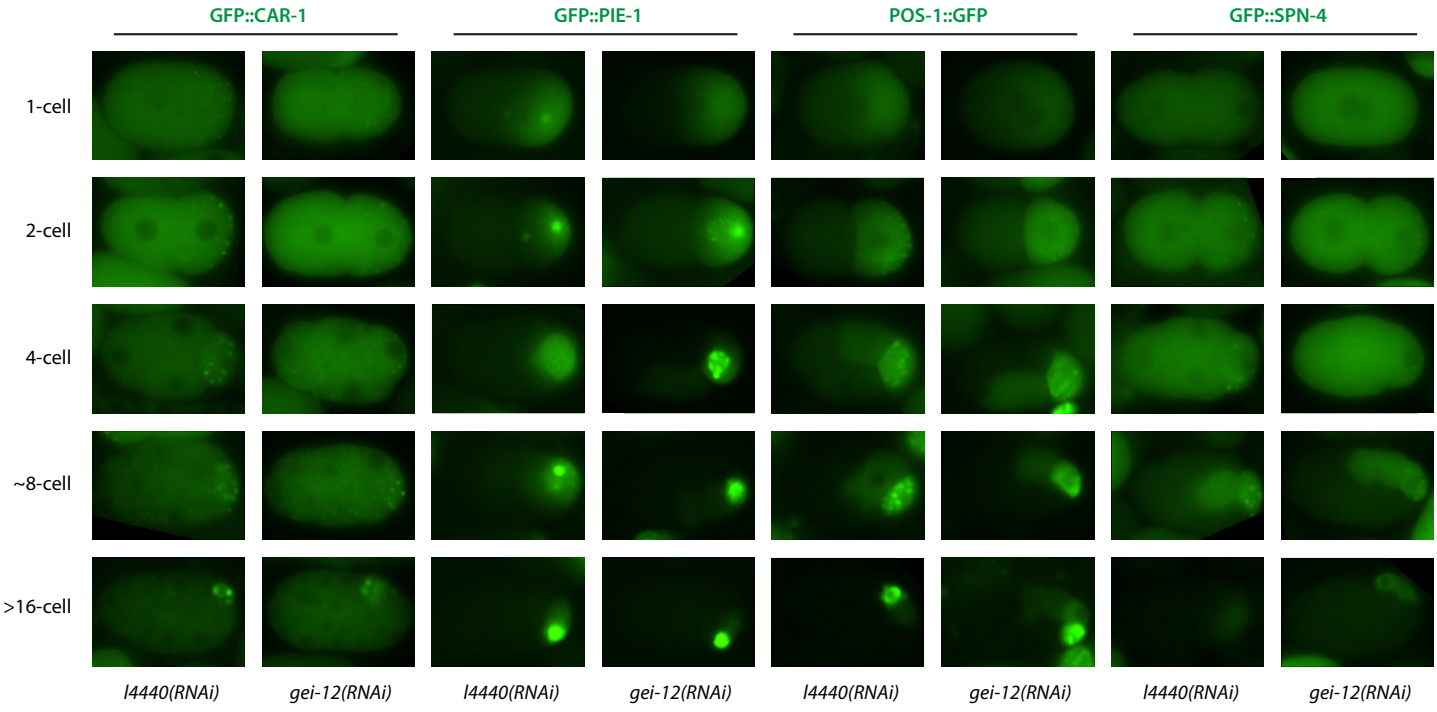
GFP::CAR-1
GFP::PIE-1
POS-1::GFP
GFP::SPN-4
1-cell
2-cell
4-cell
~8-cell
>16-cell
l4440(RNAi)
gei-12(RNAi)
l4440(RNAi)
gei-12(RNAi)
l4440(RNAi)
gei-12(RNAi)
l4440(RNAi)
gei-12(RNAi)

# Figure S7

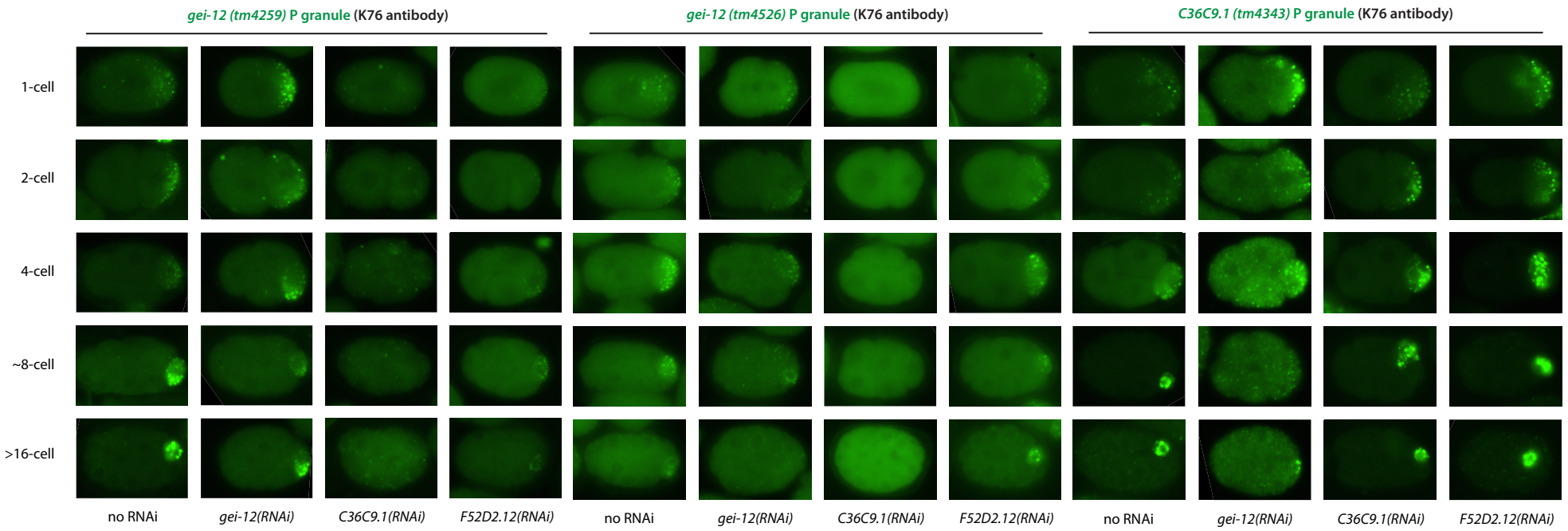
gei-12 (tm4259) P granule (K76 antibody)
gei-12 (tm4526) P granule (K76 antibody)
C36C9.1 (tm4343) P granule (K76 antibody)
1-cell
2-cell
4-cell
~8-cell
>16-cell
no RNAi
gei-12(RNAi)
C36C9.1(RNAi)
F52D2.12(RNAi)
no RNAi
gei-12(RNAi)
C36C9.1(RNAi)
F52D2.12(RNAi)
no RNAi
gei-12(RNAi)
C36C9.1(RNAi)
F52D2.12(RNAi)